Novel chemical tyrosine functionalization of adeno-associated virus improves gene transfer efficiency in liver and retina

Aurélien Leray, Pierre-Alban Lalys, Juliette Varin, Mohammed Bouzelha, Audrey Bourdon, Dimitri Alvarez-Dorta, Karine Pavageau, Sébastien Depienne, Maia Marchand, Anthony Mellet, et al.

Biomedicine & Pharmacotherapy 171 (2024) 116148

Contents lists available at ScienceDirect

Biomedicine & Pharmacotherapy

journal homepage: www.elsevier.com/locate/biopha

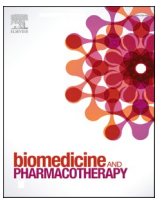

Novel chemical tyrosine functionalization of adeno-associated virus improves gene transfer efficiency in liver and retina

Aurélien Leray [a], Pierre-Alban Lalys [a], Juliette Varin [b], Mohammed Bouzelha [b], Audrey Bourdon [b], Dimitri Alvarez-Dorta [c], Karine Pavageau [b], Sébastien Depienne [a], Maia Marchand [b], Anthony Mellet [b], Joanna Demilly [b], Jean-Baptiste Ducloyer [b], Tiphaine Girard [b], Bodvaël Fraysse [b], Mireille Ledevin [d], Mickaël Guilbaud [b], Sébastien G. Gouin [a], Eduard Ayuso [b], Oumeya Adjali [b], Thibaut Larcher [d], Thérèse Cronin [b], Caroline Le Guiner [b], David Deniaud [a,*], Mathieu Mével [b,*]

[a] Nantes Université, CNRS, CEISAM, UMR 6230, F-44000 Nantes, France
[b] Nantes Université, TaRGeT, Translational Research for Gene Therapies, CHU Nantes, INSERM, UMR 1089, F-44000 Nantes, France
[c] Capacités, 26 Bd Vincent Gâche, 44200 Nantes, France
[d] INRAE, Oniris, PanTher, APEX, F-44307 Nantes, France

ARTICLE INFO

Keywords:
Adeno-associated virus
Bioconjugation
Tyrosine
Targeting
Liver
Retina

ABSTRACT

Decades of biological and clinical research have led to important advances in recombinant adeno-associated viruses rAAV-based gene therapy gene therapy. However, several challenges must be overcome to fully exploit the potential of rAAV vectors. Innovative approaches to modify viral genome and capsid elements have been used to overcome issues such as unwanted immune responses and off-targeting. While often successful, genetic modification of capsids can drastically reduce vector yield and often fails to produce vectors with properties that translate across different animal species, such as rodents, non-human primates, and humans. Here, we describe a chemical bioconjugation strategy to modify tyrosine residues on AAV capsids using specific ligands, thereby circumventing the need to genetically engineer the capsid sequence. Aromatic electrophilic substitution of the phenol ring of tyrosine residues on AAV capsids improved the *in vivo* transduction efficiency of rAAV2 vectors in both liver and retinal targets. This tyrosine bioconjugation strategy represents an innovative technology for the engineering of rAAV vectors for human gene therapy.

1. Introduction

Gene therapy with viral vectors has been used in both preclinical and clinical settings to treat cardiovascular [1], muscular [2], metabolic [3], neurological [4], hematological [5] and ophthalmological [6] diseases, as well as infectious disorders [7] and cancers[8]. Owing to their non-pathogenic nature, low immunogenicity, ease of production, and the long-term persistence of transgene expression, recombinant adeno-associated viruses (rAAV) are one of the most widely used viral vector for *in vivo* gene therapy. Several rAAV-based gene therapy products (Luxturna, Zolgensma, Roctavian, Upstaza and Hemgenix) [9–11] have been approved in Europe and the United States. rAAVs thus constitute a promising platform for the treatment of many diseases.

However, while rAAVs are effective as therapeutic gene delivery vehicles, there are several limitations to these vectors that hinder full realization of their potential. Indeed, none of the rAAVs currently used show exclusive tropism for a specific organ or tissue. The high vector doses required to achieve a therapeutic outcome in a given tissue can thus trigger an immune response that in turn can result in elimination of the transduced cells [12]. Moreover, a large proportion of the population has already been infected with wild-type AAVs and therefore expresses neutralizing anti-AAV antibodies that prevent rAAV-mediated gene transfer. This leads to exclusion of seropositive patients from experimental protocols [13] and limits the use of rAAVs in the general population.

With ever more rAAV-delivered transgenes in clinical trials, there is an unmet need for a new generation of rAAVs with greater transduction efficiency (*i.e.* increased number of transduced cells). A variety of

* Corresponding authors.
E-mail addresses: david.deniaud@univ-nantes.fr (D. Deniaud), mathieu.mevel@univ-nantes.fr (M. Mével).

https://doi.org/10.1016/j.biopha.2024.116148
Received 7 November 2023; Received in revised form 10 January 2024; Accepted 10 January 2024
Available online 16 January 2024

enhancement approaches are described in the literature, most of which involve modification of the viral capsid by genetic engineering (specifically, using rational design or directed evolution approaches) [14]. However, the development of each novel rAAV variant must be accompanied by new bioproduction, manufacturing, purification, and characterization processes.

Site-specific bioconjugation is a burgeoning field of research that enables covalent coupling of ligands (*e.g.* fluorophores, carbohydrates, polymers) to biomolecules and lysine is the most commonly used amino acid for chemical coupling [15]. Lysine residues on the rAAV surface have been previously exploited as molecular anchors for the conjugation of amine-reactive molecules. Indeed, our group has previously shown that rAAVs chemically modified with sugars promote cell-specific transduction and lead to lower levels of serum neutralizing antibodies compared with unmodified rAAVs [16–18].

Here, we describe a strategy for selective conjugation of ligands on tyrosine (Y) residues present on the surface of the rAAV capsid. The literature describes a wide range of biorthogonal click strategies that allow functionalization of the phenol side chain of Y [19]. Y-targeting is an effective means of designing a wide range of important biomolecules, including antibody-drug conjugates [20], glycovaccines [21], and PEG-conjugates [22]. Previous work has been done on the Y-bioconjugation with diazonium salts on tobacco mosaic virus by Francis and co-workers [23] and recently reviewed [24]. Nevertheless, this RNA-virus about 300300 nm size is different from rAAV vectors and has not been used for gene therapy applications. Using this Y-targeting to extend the bioconjugaison possibilities on AAV vectors can be of great interest.

Because Y residues are neutral over a wide pH range, chemical modification does not alter the overall protein charge. Several studies have described the impact of genetic replacement of a Y with a phenylalanine in the rAAV capsid sequence: this change significantly increases transduction and, in some cases, has been associated with reduced biodistribution and an absence of inflammation in transduced tissues [25–27]. These effects are due to the non-phosphorylated nature of the surface Y: this prevents ubiquitination of the rAAV capsid and consequent degradation by the proteasome. Indeed, Y phosphorylation–dephosphorylation is one of the main post-translational modifications that decreases transduction efficiency [28]. Moreover, grafted ligands would protect the virus from neutralizing antibodies, preventing them from reaching the epitopes on the surface of the capsid [16,29,30]. Furthermore, the bioconjugation step is performed on purified rAAVs, meaning that the pre-established bioprocess does not need to be altered. This strategy paves the way for the development of a new method of AAV bioconjugation.

2. Materials and methods

2.1. Materials

All chemical reagents were purchased from Acros Organics or Sigma Aldrich and were used without further purification. Rabbit polyclonal anti-AAV capsid proteins antibody (cat N° 61084) was obtained from PROGEN Biotechnik. Anti-fluorescein-AP Fab fragment antibody (cat N° 11426338910) for the detection of fluorescein-labeled lectin was obtained from Sigma-Aldrich. FITC-Soybean lectin and FITC-Concanavalin A lectin were purchased from Vector Laboratories. Reactions requiring anhydrous conditions were performed under nitrogen atmosphere. All chemically synthesized compounds were characterized by ^{1}H (400°.133 or 300.135 MHz), ^{13}C (125.773 or 75.480 MHz) NMR spectroscopy (Bruker Avance 300 Ultra Shield or Bruker Avance III 400 spectrometer). Chemical shifts are reported in parts per million (ppm); coupling constants are reported in units of Hertz [Hz]. The following abbreviations were used: s = singlet, d = doublet, t = triplet, q = quartet, quin = quintet, br = broad singlet. When needed, ^{13}C heteronuclear HMQC and HMBC were used to unambiguously establish structures. High-resolution mass spectra (HRMS) were recorded with a Thermo Fisher hybrid LTQ-orbitrap spectrometer (ESI^{+}) and a Bruker Autoflex III SmartBeam spectrometer (MALDI). HPLC analysis were performed on an HPLC autopurification system (WATERS) equipped with BGM 2545 binary pump, a 2767 Sample Manager, and an UV–visible diode array detector and evaporative light scattering detector in series (WATERS 996 PDA and WATERS 2424 ESLD). Chromatographic separation was performed on an Atlantis T3 (WATERS; 4.6 × 150 mm, 5 μ). The mobile phase consisted of water (solvent A) and acetonitrile (solvent B). Gradient mix: 0.0 min [95% A; 5% B], 20.0 min [77% A; 23% B]. Flowrate: 1 mL/min.

All chemically synthesized products were purified by flash chromatography (GRACE REVELERIS Flash Chromatography System) equipped with UV and DLS detectors.

The synthesis of compounds **1** and **8** were already published [16].

2.2. Synthesis

2.2.1. Compound 2

To a solution of ammonium salt **1** (0.73 g, 1.12 mmol, 1 eq) in DCM (25 mL) was added DMAP (0.687 g, 5.6 mmol, 5 eq), followed by 4-nitrobenzoylchloride (0.626 g, 3.36 mmol, 3 eq). The mixture was stirred for 4 h at RT. The resulting mixture was washed with HCl 1 M, water, a saturated solution of $NaHCO_3$. The organic phase was dried and concentrated under vacuum. The crude was purified by column chromatography (SiO_2 AcOEt/MeOH, 85/15 as eluent) to give the desired product **2** (0.365 g, 0.581 mmol, 52%) as a slightly yellow solid.

^{1}H NMR (300 MHz, MeOD): δ (ppm) 8.34 (d, 2 H, J = 8.98 Hz, Ar), 8.06 (d, 2 H, J = 9 Hz, Ar), 5.32 (d, 1 H, J = 3.13 Hz, H-4), 5.06 (dd, 1 H, J = 3.3 Hz, J = 11 Hz, H-3), 4.61 (d, 1 H, J = 8.41 Hz, H-1), 4.12 (m, 3 H, H-2, H-6), 3.95 (m, 2 H, H-5), 3.65 (m, 12 H), 2.10 (s, 3 H, AcO), 2.02 (s, 3 H, AcO), 1.94 (s, 3 H, AcO), 1.92 (s, 3 H, AcO). ^{13}C NMR (75 MHz, MeOD): δ (ppm) 173.6 (C, AcO), 172.1 (C, AcO), 172.0 (C, AcO), 171.7 (C, AcO), 168.2 (C, C═O), 151.0 (C, Ar), 141.4 (C, Ar), 129.8 (2 CH, Ar), 124.6 (2 CH, Ar), 102.8 (CH, C-1), 72.2 (CH, C-3), 71.8 (CH sugar), 71.6 (CH_2), 71.4 (CH_2), 71.3 (CH_2), 70.4 (CH_2), 70.2 (CH_2), 68.2 (CH, C-4), 62.7 (CH sugar), 51.6 (CH_2, C-6), 41.2 (CH_2), 22.9 (CH_3, AcO), 20.5 (2 CH_3, 2 AcO), 20.5 (CH_3, AcO). HRMS: TOF (ESI+) *m/z* calcd for $C_{27}H_{37}N_3O_{14}Na$ $[M + Na]^{+}$: 650.2173, found: 650.2172.

2.2.2. Compound 4

Compound **2** (140 mg, 0.223 mmol) was dissolved in dry MeOH (2.2 mL) and sodium methoxide (67 μL of 1 M solution in MeOH, 0.079 mmol) was added. The mixture was stirred for 2 h, and neutralized by adding acid resin Amberlite IR120 (H), filtered and the solvents evaporated to dryness. The crude of the reaction was used in the next step without further purification.

To a solution of deprotected sugar **3** in MeOH (4.4 mL) was added Pd/C (28 mg, 20% w). The resulting suspension was stirred under H_2 atmosphere (1 atm) for 4 h. The Pd/C was removed by filtration through Celite® and the filtrate was evaporated under reduced pressure. The crude of the reaction was lyophilized to yield the aniline **4** (91 mg, 0.152 mmol, 68%) as a white solid.

^{1}H NMR (400 MHz, D_2O): δ (ppm) 7.52 (d, 2 H, J = 8.8 Hz, Ar), 6.58 (d, 2 H, J = 8.8 Hz, Ar), 4.33 (d, 1 H, J = 8.4 Hz, H-1), 3.85 (m, 2 H), 3.72–3.43 (m, 17 H), 3.37 (t, 1 H, J = 5.8 Hz), 1.96 (s, 3 H, NHAc). ^{13}C NMR (100 MHz, D_2O): δ (ppm) 174.7 (C, NHAc), 170.5 (C, C═O), 150.8 (C, Ar), 129.0 (2 CH, Ar), 123.0 (C, Ar), 115.2 (2 CH, Ar), 101.6 (CH, C-1), 71.2 (CH), 75.1 (CH), 69.8 (CH_2), 69.7 (CH_2), 69.6 (CH_2), 69.0 (CH_2), 68.8 (CH_2), 67.9 (CH), 61.0 (CH_2), 52.4 (CH), 39.4 (CH_2, C-6), 22.3 (CH_3, NHAc). HRMS: TOF (ESI+) *m/z* calcd for $C_{21}H_{33}N_3O_9Na$ $[M + Na]^{+}$: 494.2114, found: 494.2108.

2.2.3. Compound 5 GalNAc(Y)

To a solution of **4** (21 mg, 0.0445 mmol, 1 eq, placed in a NMR tube) in D_2O (0.6 mL), HBF_4 (7 μL, 0.0534 mmol, 1.2 eq) and tBuONO (7 μL, 0.0534 mmol, 1.2 eq) were added and the mixture was manually shaken

for 30 s at RT. After 5 min, the quantitative conversion to diazonium salt **5** was observed by 1 H NMR. The compound **5** was prepared freshly before the bioconjugation step and then freeze-dried.

^{1}H NMR (300 MHz, D2O): δ (ppm) 8.69 (d, 2 H, $J = 9$ Hz, Ar), 8.23 (d, 2 H, $J = 9$ Hz, Ar), 4.45 (d, 1 H, $J = 8.4$ Hz, H-1), 3.74–3.64 (m, 20 H), 2.00 (s, 3 H, AcO). ^{13}C NMR (100 MHz, D_2O): δ (ppm) 174.8 (C, NHAc), 167.2 (C, C═O), 145.5 (C, Ar), 132.8 (2 CH, Ar), 130.3 (2 CH, Ar), 117.0 (C, Ar), 101.6 (CH, C-1), 71.2 (CH), 75.1 (CH), 69.7 (2 x CH_2), 69.5 (CH_2), 68.9 (CH_2), 68.6 (CH_2), 67.9 (CH), 61.0 (CH_2), 52.4 (CH), 39.9 (CH_2, C-6), 22.3 (CH_3, NHAc). HRMS: TOF (ESI+) *m/z* calcd for $C_{21}H_{31}N_2O_9$ [M - N_2]$^+$: 455.2030, found: 455.2023.

2.2.4. Compound 6

To a solution of ammonium salt **1** (0.150 g, 0.230 mmol, 1 eq) in dry DCM (15 mL), were added DMAP (0.140 g, 1.15 mmol, 5 eq), and benzoyl chloride (0.1 mL, 0.8 mmol, 3 eq). The mixture was stirred for 4 h at RT. The resulting mixture was washed with HCl 1 M, water, a saturated solution of $NaHCO_3$. The organic phase was dried and concentrated under vacuum. The crude was purified by column chromatography (SiO_2, AcOEt/MeOH, 8/2 as eluent) to give the desired product **6** (90 mg, 0.154 mmol, 67%) as a white solid.

^{1}H NMR (400 MHz, MeOD): δ (ppm) 7.83 (d, 2 H, $J = 8.4$ Hz, Ar), 7.48 (m, 3 H, Ar), 5.31 (d, 1 H, $J = 3.2$ Hz, H-4), 5.06 (dd, 1 H, $J = 11.2$ Hz, $J = 3.2$ Hz, H-3), 4.61 (d, 1 H, $J = 8.4$ Hz, H- 1), 4.11 (m, 3 H, H-2, H-6), 3.92 (m, 2 H, H-5), 3.68–3.59 (m, 12 H), 2.12 (s, 3 H, AcO), 2.02 (s, 3 H, AcO), 1.94 (s, 3 H, AcO), 1.91 (s, 3 H, AcO). ^{13}C NMR (100 MHz, MeOD): δ (ppm) 173.6 (C, AcO), 172.1 (C, AcO), 172.1 (C, AcO), 171.7 (C, AcO), 170.3 (C, C═O), 135.7 (C, Ar), 132.7 (C, Ar), 129.6 (2 CH, Ar), 128.3 (2 CH, Ar), 102.7 (CH, C-1), 72.2 (CH, C-3), 71.8 (CH, C-5), 71.6 (CH_2), 71.4 (CH_2), 71.3 (CH_2), 70.6 (CH_2), 70.1 (CH_2), 68.2 (CH, C-4), 62.7 (CH, C-2), 51.65 (CH_2, C-6), 40.9 (CH_2), 22.9 (CH_3, NHAc), 20.6 (CH_3, AcO), 20.5 (CH_3, AcO), 20.5 (CH_3, AcO). HRMS: TOF (ESI+) *m/z* calcd for $C_{27}H_{39}N_2O_{12}$ [M + H]$^+$: 583.2503, found: 583.2504.

2.2.5. Compound 7

To a solution of **6** (89 mg, 0.153 mmol, 1 eq,) in a mixture 1:1 H_2O/MeOH (20 mL) was added Amberlist basic resin (IRN 78). The mixture was stirred for 2 h at RT. The resin was filtered and the filtrate concentrated under vacuum to give the corresponding product as a colorless oil. The oil was then freeze-dried to give the desired product **7** (70 mg, 0.153 mmol, quant.) as a white solid.

^{1}H NMR (400 MHz, MeOD): δ (ppm) 7.83 (m, 2 H, Ar), 7.49 (m, 3 H, Ar), 4.42 (d, 1 H, $J = 8.4$ Hz, H-1), 3.93 (m, 2 H), 3.81–3.56 (m, 16 H), 3.46 (m, 1 H), 1.96 (s, 3 H, AcO) ^{13}C NMR (100 MHz, MeOD): δ (ppm) 174.1 (C, AcO), 170.4 (C, C═O), 135.7 (C, Ar), 132.6 (C, Ar), 129.6 (2 CH, Ar), 128.3 (2 CH, Ar), 103.1 (CH, C-1), 76.7 (CH), 73.5 (CH), 71.6 (CH_2), 71.6 (CH_2), 71.4 (CH_2), 70.6 (CH_2), 69.7 (CH_2), 69.7 (CH), 62.5 (CH), 54.3 (CH_2), 40.9 (CH_2), 23.1 (CH_3, NHAc). HRMS: TOF (ESI+) *m/z* calcd for $C_{21}H_{32}N_2O_9Na$ [M + Na]$^+$: 479.2006, found: 479.1997.

2.2.6. Compound 9

To a solution of ammonium salt **8** (0.900 g, 1.38 mmol, 1 eq) in DCM, were added DMAP (0.506 g, 4.14 mmol, 3 eq) and 4-nitrobenzoylchloride (0.769 g, 4.14 mmol, 3 eq). The mixture was stirred at RT for 4 h. The organic solution was washed with HCl 1 M, water, a saturated solution of NaHCO3. The organic phase was dried and concentrated under vacuum. The crude was purified by column chromatography (SiO2, AcOEt/MeOH, 85/15 as eluent) to give the desired product **9** (0.27 g, 0.43 mmol, 31%) as a slightly yellow solid.

^{1}H NMR (300 MHz, CDCl3): δ (ppm) 8.27 (m, 2 H, Ar), 7.99 (m, 2 H, Ar), 7.19 (br s, 1 H), 5.29 (m, 3 H, H-2, H-3, H-4), 4.86 (d, 1 H, $J = 1.62$ Hz, H-1), 4.25 (m, 1 H, H-6), 4.07 (m, 2 H), 3.87- 3.66 (m, 13 H, H-5, H-6, PEG), 2.15 (s, 3 H, AcO), 2.09 (s, 3 H, AcO), 2.03 (s, 3 H, AcO), 1.98 (s, 3 H, AcO). ^{13}C NMR (75 MHz, CDCl3): δ (ppm) 170.8 (C, AcO), 170.3 (C, 2 AcO), 169.8 (C, AcO), 165.6 (C, C═O), 149.7 (C, Ar), 140.4 (C, Ar), 128.5 (2 CH, Ar), 123.8 (2 CH, Ar), 97.8 (CH, C-1), 70.8 (CH_2), 70.4 (CH_2), 70.1 (CH_2), 69.8 (CH, sugar), 69.7 (CH, sugar), 68.7 (CH_2), 67.5 (CH_2), 66.2 (CH, sugar), 62.6 (CH_2, C-6), 40.2 (CH_2), 21.0 (CH_3, AcO), 20.9 (CH_3, AcO), 20.8 (2 CH_3, AcO). HRMS: TOF (ESI+) *m/z* calcd for $C_{27}H_{36}N_2O_{15}Na$ [M + Na]$^+$: 651.2013, found: 651.2002.

2.2.7. Compound 11

Compound **9** (124 mg, 0.197 mmol) was dissolved in dry MeOH (2.8 mL) and sodium methoxide (79 μL of 1 M solution in MeOH, 0.079 mmol) was added. The mixture was stirred for 2 h, and neutralized by adding acid resin Amberlite IR120 (H), filtered and the solvents evaporated to dryness. The crude of the reaction was used in the next step without further purification.

To a solution of deprotected sugar in MeOH **10** (3 mL) was added Pd/C (25 mg, 20% w). The resulting suspension was stirred under H_2 atmosphere (1 atm) for 4 h. The Pd/C was removed by filtration through Celite® and the filtrate was evaporated under reduced pressure. The crude of the reaction was lyophilized to yield the aniline **11** (69 mg, 0.160 mmol, 81%) as a white solid.

^{1}H NMR (400 MHz, CD_3OD): $\delta = 3.52$–3.68 (m, 14 H), 3.69–3.74 (m, 2 H), 3.78–3.85 (m, 3 H), 6.67 (d, 2 H, $J = 8.8$ Hz, Ar), 7.71 (d, 2 H, $J = 8.8$ Hz, Ar). ^{13}C NMR (100.6 MHz, CDCl3): $\delta = 40.7$ (CH_2), 62.9 (CH_2, C-6), 68.6 (CH), 70.8 (CH_2), 71.28 (CH_2), 71.32 (CH_2), 71.37(CH_2), 71.5 (CH), 72.1 (CH), 72.6 (CH), 74.6 (CH), 101.7 (CH, C-1), 114.8 (2 x CH, Ar), 123.2 (C, Ar), 129.9 (2 x CH, Ar), 153.1 (C, Ar),170.2 (C, amide). HRMS (ESI): *m/z* calcd for $C_{19}H_{30}N_2O_9Na$ [M + Na]$^+$: 453.1849, found: 453.1841.

2.2.8. Compound 12 Man(Y)

To a solution of **11** (10 mg, 0.0232 mmol, 1 eq, placed in a NMR tube) in D_2O (0.6 mL), HBF_4 (3.5 μL, 0.0278 mmol, 1.2 eq) and tBuONO (3.7 μL, 0.0278 mmol, 1.2 eq) were added and the mixture was manually shaken for 30 s at RT. After 5 min, the quantitative conversion to diazonium salt **12** was observed by 1 H NMR. The compound **12** was prepared freshly before the bioconjugation step and then freeze-dried.

^{1}H NMR (400 MHz, D_2O): $\delta = 3.68$–3.85 (m, 15 H), 3.88–3.94 (m, 2 H), 3.97 (dd, 1 H, $J = 3.5$ Hz, $J = 1.8$ Hz, H-2), 4.90 (d, 1 H, $J = 1.7$ Hz, H-1), 8.30 (d, 2 H, $J = 9.0$ Hz, Ar), 8.80 (d, 2 H, $J = 8.8$ Hz, Ar). ^{13}C NMR (100.6 MHz, D_2O): $\delta = 40.0$ (CH_2), 48.9 (CH), 60.9 (CH_2), 66.4 (CH_2, C-6), 66.8 (CH), 68.6 (CH_2), 69.5 (2 x CH_2), 69.7 (CH_2), 70.0 (CH), 70.5 (CH), 72.8 (CH), 99.9 (CH, C-1), 117.0 (C, Ar), 130.3 (2 x CH, Ar), 132.8 (2 x CH, Ar), 145.5 (C, Ar), 167.2 (C, amide).

2.2.9. Compound 13

To a solution of ammonium salt **8** (0.230 g, 0.353 mmol, 1 eq) in dry DCM, were added DMAP (0.129 g, 1.05 mmol, 3 eq) and 4-nitrobenzoylchloride (0.194 g, 1.05 mmol, 3 eq). The mixture was stirred for 4 h at RT. The resulting mixture was washed with HCl 1 M, water and a saturated solution of $NaHCO_3$. The organic phase was dried and concentrated under vacuum. The crude was purified by column chromatography (SiO_2, AcOEt/MeOH, 85/15 as eluent) to give the desired product **13** (70 mg, 0.120 mmol, 34%) as a slightly yellow solid.

^{1}H NMR (400 MHz, MeOD): δ (ppm) 7.82 (m, 2 H, Ar), 7.49 (m, 3 H, Ar), 5.26 (m, 3 H, H2, H3, H4), 4.87 (d, 1 H, $J = 1.36$ Hz, H-1), 4.23 (dd, 1 H, $J = 5$ Hz, $J = 12$,3 Hz, H-6), 4.10 (m, 2 H, H-5, H-6), 3.82 (m, 1 H), 3.71–3.58 (m, 12 H), 2.12 (s, 3 H, AcO), 2.05 (s, 3 H, AcO), 2.02 (s, 3 H, AcO), 1.95 (s, 3 H, AcO). ^{13}C NMR (100 MHz, MeOD): δ (ppm) 172.3 (C, AcO), 171.5 (C, AcO), 171.5 (C, AcO), 171.4 (C, AcO), 170.2 (C, AcO), 135.7 (C, Ar), 132.6 (CH, Ar), 129.5 (2 CH, Ar), 128.3 (2 CH, Ar), 98.9 (CH, C-1), 71.6 (CH_2), 71.3 (CH_2), 71.2 (CH_2), 70.7 (CH, sugar), 70.7 (CH, sugar), 70.6 (CH, sugar), 69.8 (CH, C-5), 68.3 (CH_2), 67.3 (CH_2), 63.6 (CH_2, C-6), 40.9 (CH_2), 20.6 (CH_3, AcO), 20.6 (CH_3, AcO), 20.6 (CH_3, AcO), 20.5 (CH_3, AcO). HRMS: TOF (ESI+) *m/z* calcd for $C_{27}H_{38}N0_{13}$ [M + H]$^+$: 584.2343, found: 584.2344.

2.2.10. Compound 14

To a solution of **13** (70 mg, 0.120 mmol, 1 eq) in a mixture 1:1 H_2O/

MeOH (10 mL) was added Amberlist basic resin (IRN 78). The mixture was stirred 2 h at RT. The resin was filtered and the filtrate concentrated under vacuum to give the desired product **14** (50 mg, 0.120 mmol, quant.) as a white solid.

^{1}H NMR (400 MHz, D2O): δ (ppm) 7.84 (m, 2 H, Ar), 7.69 (m, 1 H, Ar), 7.60 (m, 2 H, Ar), 4.88 (d, 1 H, J = 1.7 Hz, H-1), 3.97 (m, 1 H), 3.93–3.63 (m, 18 H). ^{13}C NMR (100 MHz, D2O): δ (ppm) 171.1 (C, C═O), 133.6 (C, Ar), 132.2 (CH, Ar), 128.8 (2 CH, Ar), 127.1 (2 CH, Ar), 99.9 (CH, C-1), 72.7 (CH, sugar), 70.5 (CH, sugar), 69.9 (CH, sugar), 69.6 (CH_2), 69.6 (CH_2), 68.9 (CH_2), 66.7 (CH, sugar), 66.4 (CH_2), 60.9 (CH_2), 39.5 (CH_2). HRMS: TOF (ESI+) *m/z* calcd for $C_{19}H_{29}NO_9Na$ [M + Na]$^{+}$: 438.1740, found: 438.1730.

2.3. AAV2 production and purification

AAV2 vectors were produced from two plasmids: (i) pHelper, PDP2-KANA encoding AAV Rep2-Cap2 and adenovirus helper genes (E2A, VA RNA, and E4); and (ii) the pVector ss-CAG-eGFP containing the ITRs. All vectors were produced by transient transfection of HEK293 cells using the calcium phosphate-HeBS method. AAV2 transfected cells were harvested 48 h after transfection and treated with Triton-1% and benzonase (25 U/mL) for 1 h at 37 °C. The resulting bulk was subjected to freeze-thaw cycles to release vector particles. The cellular debris were removed by centrifugation at 2500 rpm for 15 min. Cell lysates were precipitated with PEG overnight and clarified by centrifugation at 4000 rpm for 1 h. The precipitates were then incubated with benzonase for 30 min at 37 °C and collected after centrifugation at 10,000 g for 10 min at 4 °C. Vectors were purified by double cesium chloride (CsCl) gradient ultracentrifugation. The viral suspension was then subjected to four successive rounds of dialysis with mild stirring in a Slide-a-Lyzer cassette (Pierce) against dPBS (containing Ca^{++} and Mg^{++}).

2.4. Bioconjugation and purification

AAV2-GFP ($1^{E}12$ vg, 2.49 nmol) were added to a solution of TBS buffer (pH 9.3) containing compounds **5, 7, 12 or 14** ($3^{E}5$ equivalents), as stated in the respective results sections, and incubated for 4 h at RT. The solutions containing the vectors were then dialyzed against dPBS + 0.001% Pluronic to remove free molecules that had not bound to the AAV capsid.

2.5. Titration of AAV vector genomes

A total of 3 μL of AAV was treated with 20 units of DNase I (Roche #04716728001) at 37 °C for 45 min to remove residual DNA in vector samples. After treatment with DNase I, 20 μL of proteinase K (20 mg/mL; MACHEREY-NAGEL # 740506) was added and the mixture incubated at 70 °C for 20 min. An extraction column (NucleoSpin®RNA Virus) was then used to extract DNA from purified AAV vectors.

Quantitative real time PCR (qPCR) was performed with a StepOnePlus™ Real-Time PCR System Upgrade (Life Technologies). All PCRs were performed with a final volume of 20 μL, including primers and probes targeting the ITR2 sequence, PCR Master Mix (TaKaRa), and 5 μL of template DNA (plasmid standard or sample DNA). qPCR was carried out with an initial denaturation step at 95 °C for 20 s, followed by 45 cycles of denaturation at 95 °C for 1 s and annealing/extension at 56 °C for 20 s. Plasmid standards were generated with seven serial dilutions (containing 10^{8} to 10^{2} plasmid copies), as described by D'Costa *et al.* [31].

2.6. Western blot and silver staining

All vectors were denatured at 100 °C for 5 min using Laemmli sample buffer and separated by SDS-PAGE on 10% Tris-glycine polyacrylamide gels (Life Technologies). Precision Plus Protein All Blue Standards (BioRad) were used as a molecular-weight size marker. After electrophoresis, gels were either silver stained (PlusOne Silver Staining Kit, Protein; GE Healthcare) or transferred onto nitrocellulose membranes for Western blot. After transferring the proteins to nitrocellulose membrane using a transfer buffer (25 mM Tris/192 mM glycine/0.1 (w/v) SDS/20% MeOH) for 1 h at 150 mA in a Trans-Blot SD Semi-Dry Transfer Cell (Bio-Rad), the membrane was saturated for 2 h at RT with 5% semi-skimmed milk in PBS-Tween (0.1%) or with 1% gelatin, 0.1% Igepal in PBS-Tween (0.01%). After saturation, the membrane was probed with the corresponding antibody (anti-capsid polyclonal, B1 monoclonal, or anti-fluorescein-AP) and FITC-Soybean lectin (GalNAc detection) or FITC-Concanavalin A lectin (mannose detection) overnight at 4 °C. Three washes (15 min at RT) with PBS-Tween (0.1%) were performed between each stage to remove unbound reagents. Bands were visualized by chemiluminescence using alkaline phosphatase (AP) or horseradish peroxidase (HRP)-conjugated secondary antibodies and captured on X-ray film.

2.7. Dynamic light scattering

Dynamic light scattering (DLS) was performed using a Malvern Zetasizer Nano ZS. Calibration was controlled beforehand using a 30 and 300 nm solution of Nanosphere Size Standard. A volume of 50 μL of each vector was placed in a specific cuvette (DTS0118; Malvern) and analyzed by volume.

2.8. 3D modelling of the capsid

Structural analysis was performed using the PyMOL Molecular Graphics System, Version 1.8, Schrödinger, LLC. AAV2 crystal structure was obtained from the Protein Data Bank (PDB ID: 1LP3). The viral capsid was reconstituted from the monomer crystal structure using the *BiologicalUnit/Quat* script (https://pymolwiki.org/index.php/BiologicalUnit/Quat). The analysis of surface-exposed tyrosine residues was performed on a single monomer, surrounded by seven adjacent monomers (one, two and four from the 2-fold, 3-fold and 5-fold symmetry axis, respectively), using the *findSurfaceResidues* script (https://pymolwiki.org/index.php/ FindSurfaceResidues), with a solvent-exposure cut-off value of 5 Å. Tyrosine residues located on the internal capsid surface were identified *via* manual inspection and discarded, resulting in the list of surface-exposed tyrosine residues represented in this paper.

2.9. Transduction of HEK cells

HEK293 Cells were seeded in a 24-well plate at adensity of approximately $1.5^{E}5$ cells/well.

After 24 h, the cells were transduced at MOI of 10^{4} with AAV2 or chemically modified AAV2 vectors in 0.5 mL of culture medium. 6 h after the transduction, 0.5 mL of fresh culture medium was added to each well. All AAV vectors encoded for GFP.

The percentage of GFP positive cells was measured by FACS analysis 48 h after the transduction. Cells were dissociated with Trypsin-EDTA (Sigma-Aldrich), fixed with 4% paraformaldehyde and analysed on a BD-LSRII Flow Cytometer (BD Bioscience). All data were processed by FlowJo (V10; Flowjo LLC, Ashland, OR).

2.10. Transduction of primary mouse hepatocytes

Primary mouse hepatocytes and culture medium were purchased from BIOPREDIC international (Rennes, FRANCE). Mouse hepatocytes were seeded in a 24-well plate at a density of approximately $2.5^{E}5$ cells/well. After reception, cell culture medium was removed and replaced with 1 mL of basal medium (MIL600) with additives (ADD222) and incubated 2 h at 37 °C and 5% CO_2. Primary mouse hepatocytes were transduced at MOI of 10^{5} with AAV2 or AAV2-GalNAc(Y) vectors in 0.5 mL of culture medium. 6 h after the transduction, 0.5 mL of fresh culture medium was added to each well. All AAV vectors encoded for GFP. The

percentage of GFP positive cells was measured by FACS analysis 72 h after the transduction. Cells were dissociated with Trypsin-EDTA (Sigma-Aldrich), fixed with 4% paraformaldehyde and analysed on a BD-LSRII Flow Cytometer (BD Bioscience). All data were processed by FlowJo (V10; Flowjo LLC, Ashland, OR).

2.11. AAV infectious titer measurements

The infectivity of each sample was measured as follows. HEK293 were seeded in 2 mL DMEM growth medium in 6-well culture plates at a density of 1^E6 cells/well. Cells were then incubated overnight at 37 °C to reach 50% confluence. The viral stock was then diluted 10-fold by serial dilution. Next, 2 μL of each dilution was added to separate wells in the 6-well plates. Plates were then incubated at 37 °C for 24 h. The infectivity of the AAV2-GFP control was measured immediately upon thawing of the sample. The same procedure was used for mannose particles. AAV-GFP-infected cells were detected by fluorescence microscopy.

The transducing unit (TU) titer was calculated using the following formula:

$$TU/mL = (4040 \times NGFP \times dilutions \times 1000)/V$$

where NGFP is the mean number of GFP-positive cells per well and V is the volume (in μL) of vector used to infect cells.

2.12. Animal care and walfare

Experiments were performed on C57BL/6 (B6) mice. Animals were euthanized 1 month after AAV injection. Research was conducted at the UTE IRS2 (University of Nantes, France) for the liver study, and at the Boisbonne Centre (ONIRIS, Nantes-Atlantic College of Veterinary Medicine, Nantes) for the retina study. The Institutional Animal Care and Use Committee of the Région des Pays de la Loire as well as the French Ministry for National Education, Higher Education and Research approved the protocols (authorizations #29288 and #H30285). Animals were randomly assigned to the different experimental groups. They were sacrificed by intravenous injection of pentobarbital sodium (Dolethal; Vetoquinol) in accordance with approved protocols.

2.13. Intravenous injection

Mice were injected intravenously (i.v.) with a dose of 5^E12 vg/kg of either AAV2-GalNAC(Y) eGFP-expressing or unmodified AAV2 eGFP-expressing. Eight weeks old C57BL/6 (B6) mice (Charles River Laboratories) were used in this study. 3 groups were formed, 6 mice per group.

Administration of chemically modified AAV2 vectors (or formulation buffer) by IV injection through the caudal tail vein, under general anesthesia. Mice were injected intravenously (i.v.) with a dose of 5^E12 vg/kg.

The blood samples will be taken on the day of the injection, after every two weeks up to one-month post injection. All animals will be euthanized one-month after injection, samples were collected in particular blood, liver, spleen, muscle, heart, kidney and lung.

2.14. Absolute quantification of vector genomes by qPCR in mice tissue samples

Liver samples were obtained just after sacrifice in conditions that minimized cross contamination and avoided qPCR inhibition, as described by Le Guiner et al. [32]. Samples were snap-frozen in liquid nitrogen and stored at ≤ -70 °C before DNA extraction. gDNA was extracted using Gentra Puregene kit (Qiagen) and TissueLyser II (Qiagen), according to the manufacturer's instructions. qPCR analyses were conducted on a C1000 touch thermal cycler (Bio-Rad) using 50 ng of gDNA in duplicate and premix Ex taq (Ozyme). Vector genome copy number was determined using the following primer/probe combination, designed to amplify a specific region of the *GFP* sequence present in the transgene (Forward, 5'- AGTCCGCCCTGAGCAAAGA-3'; Reverse, 5'-GCGGTCACGAACTCCAGC −3'; Probe, 5'-FAM- CAACGA-GAAGCGCGATCACATGGTC-TAMRA-3'). Endogenous gDNA copy number was determined using a primer/probe combination designed to amplify the rmurine *Hprt1* gene (Forward, 5'- TCTGTAAGAA-GGATTTAAAGAGAAGCTA-3'; Reverse, 5'- ATCACATGTTTATTCCA-CTGAGCAA-3'; Probe, 5'-FAM- AGCTCTCGATTTCCTATCAGTAACAGC -TAMRA-3'). For each sample, cycle threshold (Ct) values were compared with those obtained with different dilutions of linearized standard plasmids (containing either the *eGFP* expression cassette or the murine *Hprt1* gene). The absence of qPCR inhibition in the presence of gDNA was determined by analyzing 50 ng genomic DNA (gDNA) extracted from tissue samples from a control animal and spiked with different dilutions of standard plasmid. Results are expressed as vector genome copy number per diploid genome (vg/dg). The lower limit of quantification (LLOQ) of our test was 0.006 vg/dg. GraphPad Prism 9 software was used for statistical analysis. The nonparametric Mann Whitney test was used.

2.15. Relative quantification of GFP expression by RT-qPCR in mice tissue samples

Total RNA was extracted from snap-frozen liver, heart, skeletal muscle, lung, spleen and kidney, using Qiazol reagent (Qiagen) and treated with ezDNAse kit (Thermo Fisher Scientific), according to the manufacturer's instructions. Then, 500 ng of this RNA was reverse transcribed using Superscript IV Vilo kit (Thermo Fisher Scientific), according to the manufacturer's instructions. qPCR analysis was then performed on cDNA (diluted 1/20) using the same *GFP* primers and probe as for the quantification of transgene copy number by qPCR. *Hprt1* messenger was also amplified as an endogenous control. For each RNA sample, the absence of DNA contamination was confirmed by analysis of "cDNA-like samples" obtained without adding reverse transcriptase to the reaction mix. The absence of qPCR inhibition in the presence of cDNA was determined by analyzing cDNA obtained from tissue sample from a control animal, spiked with different dilutions of a standard plasmid. Results were expressed in relative quantification (RQ): $RQ = 2^{-\Delta Ct} = 2^{-(Ct\ GFP\ -\ Ct\ HPRT1)}$. The lower limit of quantification (LLOQ) of our test was 0.0004. GraphPad Prism 9 software was used for statistical analysis. Non-parametric Mann Whitney test was used. Samples were considered significantly different if $^*p < 0.05$, $^{**}p < 0.01$, $^{***}p < 0.001$.

2.16. Western blot and GFP expression

Total proteins were extracted from snap-frozen liver using RIPA buffer (Tris 10 mM pH 7.5; NaCl 150 mM; EDTA 1 mM; NP40 1%; sodium deoxycholate 0.5%; SDS 0.1%) containing protease inhibitor cocktail (Sigma-Aldrich). 25 μg of total protein extract were prepared in Laemmli buffer + 200 mM final of DTT, reduced 10 min at 70 °C and then loaded into a Novex 10% Tris-glycine gel (Thermo Fisher Scientific). Proteins were transferred on silica membrane using the trans-blot turbo kit (Biorad), according to the manufacturer's instructions. Membranes were blocked in 5% skim milk, 1% NP40 (Sigma-Aldrich) in TBST (Tris-buffered saline, 0.1% Tween-20) and hybridized with an anti-GFP antibody (1:8000, JL-8, Takarabio) and with a secondary anti-mouse IgG HRP-conjugated antibody (1:5000, Dako P0447). For protein loading control, the same membrane was also hybridized with an anti-mouse GAPDH antibody (1:2000, Novus IMG3073) and with a secondary anti-goat IgG HRP-conjugated antibody (1:2000, Dako P0449). Immunoblots were visualized by ECL Chemiluminescent analysis system. Semi-quantification of GFP protein expression relative to mouse GAPDH was obtained by densitometry analysis, using the ImageQuant software.

2.17. Immunohistochemistry GFP staining in mice

Formalin-fixed paraffin embedded liver samples were cut into 4 μm thick slices. Sections were first deparaffinized in methylcyclohexan and then rehydrated using decreasing concentrations of ethanol. Antigen unmasking was further performed through incubation in citrate buffer pH= 6 (40 min, 98 °C). After a permeabilization step (10 min, RT) with Triton (0.2%; VWR International, Leuven, Belgium), and a saturation step (45 min, RT) with goat serum (2%; Abcam Inc., Cambridge, MA, USA) and bovine serum albumin (5%, Sigma, St. Louis, USA), sections were then incubated (over-night, 4 °C) with a mouse monoclonal antibody against GFP (1:100; JL8 clone, Thermo Fisher Scientific, Geel, Belgium). After PBS-washing, sections were incubated with an Alexa fluor 555-conjugated goat anti-murine antibody (1:300, 1 h, RT, InVitroGen, Carlsbad, CA, USA) before washing, nuclei counterstaining with DAPI (1:1000, InVitroGen) and mounting. Whole histological preparations were digitized using fluorescence detection (Zeiss Axioscan Z1, x10 magnification). Numbers of total nuclei and positive cells based on red fluorescence were counted using QuPath software (Bankhead, P. et al. Scientific Reports, 2017) on 3 randomly selected field (2 mm^2 each) enabling to observe a mean of 17882 nuclei per sample.

2.18. Subretinal injection

Mice were anesthetized by intraperitoneal injection of ketamine/xylazine (Imalgène1000 80 mg/kg / Rompun 2% 10 mg/kg). Pupils were dilated with 0.5% tropicamide and 10% neosynephrine eye drops. Local anesthesia was achieved using 0.4% oxybuprocaïne eye drops. A vector solution of 5^E11vg/mL was prepared with 1/1000 of fluorescein dye to monitor bleb size. Under an operating microscope, 1.5 μL of vector solution was injected to the mice subretinal space by a transscleral/transchoroidal approach using a 33 G Nanofil needle and a 10 μL Nanofil syringe. Injection success was confirmed by fundus imaging immediately after injection (Spectralis® imaging system; Heidelberg Engineering Inc.).

2.19. Retinal imaging

One-month post-injection, mice were anesthetized by intraperitoneal injection of ketamine/xylazine (Imalgène1000 80 mg/kg / Rompun 2% 10 mg/kg). Pupils were dilated with 0.5% tropicamide and 10% neosynephrine eye drops. Prior to euthanasia, eye funduscopy was performed to monitor retinal appearance and GFP fluorescence (shown as white dots on images) was detected by the Spectralis® HRA imaging system (Heidelberg Engineering Inc.).

2.20. Retinal flatmounts

Mice were euthanized by cervical dislocation and then eyes were removed. Ocular globes were fixed in 4% PFA for one hour and then placed in PBS1X until dissection. Retinas were carefully dissected in PBS1X and stained with 1/1000 DAPI for 10 min. Finally, they were flatmounted on glass slides using ProlongGold Antifade mounting medium (ThermoFisher Scientific, Waltham, MA, USA). Fluorescence images of retinal flatmounts were acquired with a confocal microscope (A1 RSi, Nikon, Japan). Images for figures were handled with the Image J Software.

3. Results and discussion

Among the different Y bioconjugation reactions, we specifically focused on the diazo-coupling reaction. In this reaction, aryldiazonium salts, prepared from the corresponding aniline by the action of a nitrite in an acidic medium, establish an azo linkage with the phenol side ring of Y *via* electrophilic aromatic substitution [33]. We used two targeting ligands with a reactive diazonium salt coupling function to chemically modify the rAAV2 capsid (Fig. 1). The first carries a *N*-acetylgalactosamine (GalNAc) (Fig. 1**-A**), a sugar that serves as an asialoglycoprotein receptor (ASGPr) targeting unit for specific liver delivery [34]; and the second a mannose sugar (Man) (Fig. 1**-B**). Indeed, this second sugar has been previously used for retinal applications after lysine bioconjugation on rAAV2, with promising results [35].

Before beginning our experiments, we estimated the number of Y residues present on the capsid surface, and therefore the number of reactive functions available for chemical modification. Using rAAV2 crystallographic data and the PyMOL Molecular Graphics System, we found a total of 360 potentially accessible Y residues available for covalent coupling on the rAAV2 capsid. Next, to target the liver, we designed two GalNAc ligands (Fig. 1**-A**): compound **1,** which has a spacer at the anomeric position carrying the reactive diazonium function to perform the coupling; and compound **2**, which lacks a coupling function and is designed to validate the formation of a covalent bond and rule out the possibility of the physical adsorption of the molecule on the rAAV2 surface. Diazonium salt **1** was synthesized in 4 steps (**Scheme S-1**) from a protected GalNAc ammonium salt which reacted, in basic medium, with 4-nitrobenzoyl chloride. The hydroxyl groups of GalNAc were deprotected with the basic resin IRN78, and the nitro function was reduced to yield the corresponding aniline. Finally, 1.2 equivalents of tetrafluoroboric acid were added at room temperature, followed by 1.1 equivalents of *tert*-butylnitrite, which, after 5 min of stirring, yielded diazonium **1** in quantitative yield. This final product was used directly for the AAV bioconjugation step. Control compound **2** was prepared in two steps (**Scheme S-8**) from the corresponding ammonium salt through the action of DMAP and benzoyl chloride followed by reaction on IRN78 basic resin to cleave the acetyl groups.

To target the retina, we used a mannose-derived ligand to generate rAAV2-Man(Y), as mannose receptor is expressed on retinal pigment epithelium [36]. It has also been described that the coupling of a mannose residue on a pepsatin protein increase the solubility of the bioconjugated protein. Then, we hypotheses that this coupling on AAV capsid can also increase its hydrosolubility and its diffusion in the retina. Two mannose ligands (Fig. 1**-B**) were synthesized using the same protocol described for the GalNAc ligands (**Fig. S-13,20**). Compound **3** carried the reactive diazonium function to perform the coupling and control compound **4** lacked a coupling function (Fig. 1**-B**). All chemical compounds were characterized by NMR, HPLC, and mass spectroscopy (**Fig. S-2 to S-24**).

Bioconjugation of compounds **1** and **3** on the rAAV capsid surface was performed in the conditions described in Fig. 2A. These two ligands were used in excess (3^E5 equivalents) to avoid the possible decomposition of the diazonium salt in aqueous buffer. Aromatic electrophilic substitution of the phenol of Y was performed at room temperature for 4 h in TBS buffer at pH 9.3. Compounds **2** and **4** were used as negative controls. After titration of the samples, dot blot analysis with A20 antibody, which detects the assembled capsid, indicated that the coupling conditions were not deleterious to the rAAV capsid (Fig. 2B-C). Moreover, using soybean lectin, which recognizes the GalNAc motif, and concanavalin A, which recognizes the mannose motif, positive dots were observed only for GalNAc(Y) (**1**) and Man(Y) (**3**), which unambiguously confirmed the formation of a covalent diazo linkage between the Y phenol and the diazonium salt (Fig. 2**-B,C**).

We also confirmed these results by western blot using a polyclonal antibody and silver staining, which revealed that the three VP capsid subunits remained intact (VP3 = 61, VP2 = 73 and VP1 = 87 kDa). It is worth noting the appearance of high molecular weight bands with low intensity after grafting of the GalNAc(Y) and Man(Y) ligands onto the capsid (Fig. S25**-A,C and S26-A,C**). Western blot analysis using soybean lectin and concanavalin A indicated that covalent coupling on all three AAV capsid proteins (VP1, VP2 and VP3) occurred only with the GalNAc (Y) and Man(Y) ligands. This confirms that the aryldiazonium function was essential for Y bioconjugation (Fig. S25**-B, 26-B**).

Dynamic light scattering (DLS) also revealed the absence of particle

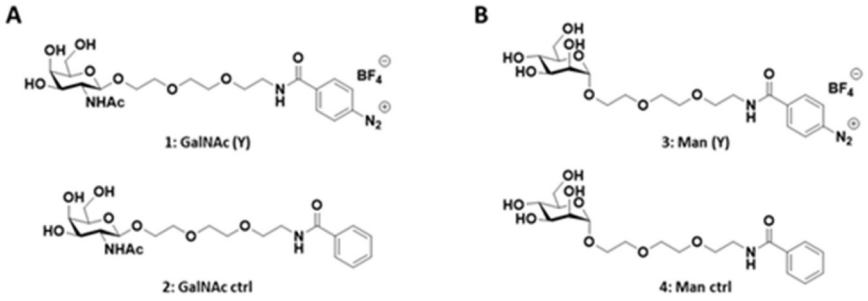

Fig. 1. Structure of the GalNAc(Y) and Man(Y) ligands used for bioconjugation on the rAAV2 capsid.

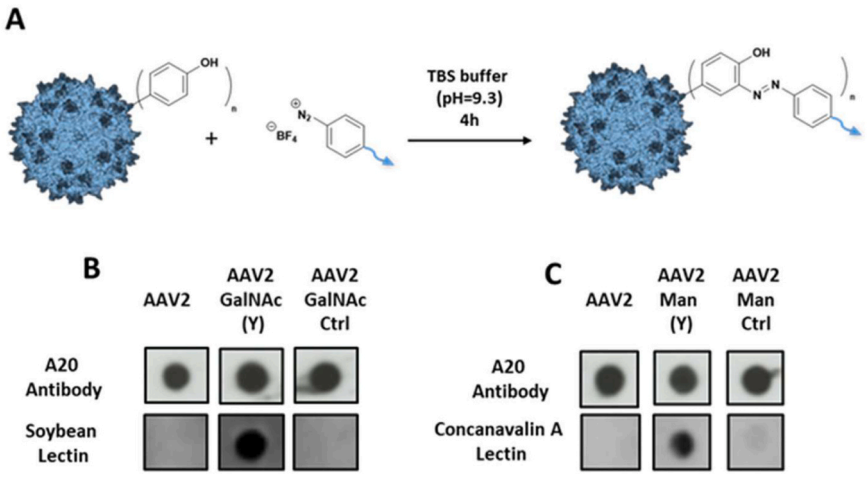

Fig. 2. A) Chemical reaction between rAAV2 and diazonium salt ligand. B) Dot blot analyses with A20 antibody (assembled capsid detection, top) and soybean lectin (GalNAc detection, bottom). C) Dot blot analyses with A20 antibody (assembled capsid detection, top) and concanavalin A lectin (mannose detection, bottom).

aggregation after coupling. Indeed, the size of rAAV2, rAAV2-GalNAc(Y) and rAAV2-Man(Y) remained around 26 nm.

For *in vitro* evaluation of the biological efficiency of the rAAV2-GalNAc(Y), which carries the eGFP transgene under the control of a CAG promoter, two different cell lines were transduced. Because GalNAc sugar allows targeting of the asialoglycoprotein receptor (ASGP-R), which is highly expressed on hepatocytes, murine primary hepatocytes were used as ASGP-R positive cells and HEK293 cells as negative controls [37]. In HEK293 cells, transduction was approximately two times more efficient for rAAV2 (90% of GFP+ cells) *versus* rAAV2-GalNAc(Y) (50% of GFP+ cells) at the same multiplicity of infection (MOI; 1^E4 for both vectors) (**Fig. S-27**). This can be explained by decreased recognition of rAAV2 by heparan sulfate proteoglycans after modification of its capsid surface [38]. Y bioconjugation therefore may have detargeted this vector from its natural receptor. On the other hand, in the same experiment using murine primary hepatocytes the transduction efficiency of rAAV2-GalNAc(Y) was 3-fold higher than that observed for the unmodified rAAV2 (**Fig. S-27**). These promising results unambiguously demonstrated the efficacy of the bioconjugation of GalNAc sugar on rAAV2 for *in vitro* targeting of hepatocytes. For this bioconjugaison another excess of ligand (3^E6 equivalents) was also used but the bioconjugates rAAV2-GalNAc(Y) were not infectious (data not shown). We next examined the transduction efficiency of rAAV2-GalNAc(Y) *in vivo*. To study liver transduction, healthy adult mice received an intravenous injection in the tail vein of unmodified rAAV2 or rAAV2-GalNAc(Y) (5^E12 vg/kg), both carrying the same CAG-eGFP expression cassette, while a control group was injected with buffer (n = 6 per group).

Liver samples were collected at euthanasia 1 month after vector administration for quantification of vector genome copy number by qPCR, eGFP protein expression by western blot, and the percentage of transduced cells by immunohistochemistry. Mean vector genome copy number was significantly lower in mice injected with rAAV2-GalNAc(Y) *versus* unmodified rAAV2 (0.02 vg/dg and 0.64 vg/dg, respectively; p = 0.026) (**Fig. S-28**). However, in the same liver samples, GFP protein expression was 2-fold higher in mice injected with rAAV2-GalNAc(Y) *versus* unmodified rAAV2 (mean relative expression: 181 and 779, respectively) (Fig. 3-**A**). While these differences were not statistically different owing to the heterogeneity of the data in the rAAV2 group (Fig. 3-**A and S-29**), the results strongly suggest a benefit of the modified capsid over the unmodified one to allow higher expression levels of the transgene product, as also suggested by RNA transcript levels (**Fig. S-30**). Finally, immunohistochemistry analysis showed a significantly higher percentage of GFP-positive cells in the livers of mice injected with rAAV2-GalNAc(Y) *versus* unmodified rAAV2 (mean: 16% and 5%, respectively; p = 0.026) (Fig. 3-**B**). GFP-positive hepatocytes (in red) were observed in the liver parenchyma of animals injected with rAAV2, mainly distributed as clusters close to portal tracts, with sparse GFP-positive cells detected around centro-lobular veins. By contrast, mice injected with rAAV2-GalNAC(Y) showed a broader distribution of GFP-positive cells, which were clustered around portal tracts and also detected throughout the liver parenchyma and in greater numbers around the portal vein (Fig. 3-**C**). Efficient targeting of hepatocytes is the main challenge associated with liver-directed gene therapy, and these data suggest a clear benefit of the Y modified capsid, as evidenced by broader transduction of hepatocytes in mouse liver, despite lower global vector copy numbers than those obtained with the unmodified rAAV2 in the liver tissue. Finally, we assessed levels of eGFP mRNA transcript in non-targeted tissues (*i.e.* heart, skeletal muscle [quadriceps], lung, spleen, and kidney). In all cases, we detected very limited levels of GFP transcript whatever the injected vector. With the rAAV2-GalNAc(Y) vector, eGFP transcripts were observed only in the heart, but at levels approximately 220 times lower than those observed in the liver of the

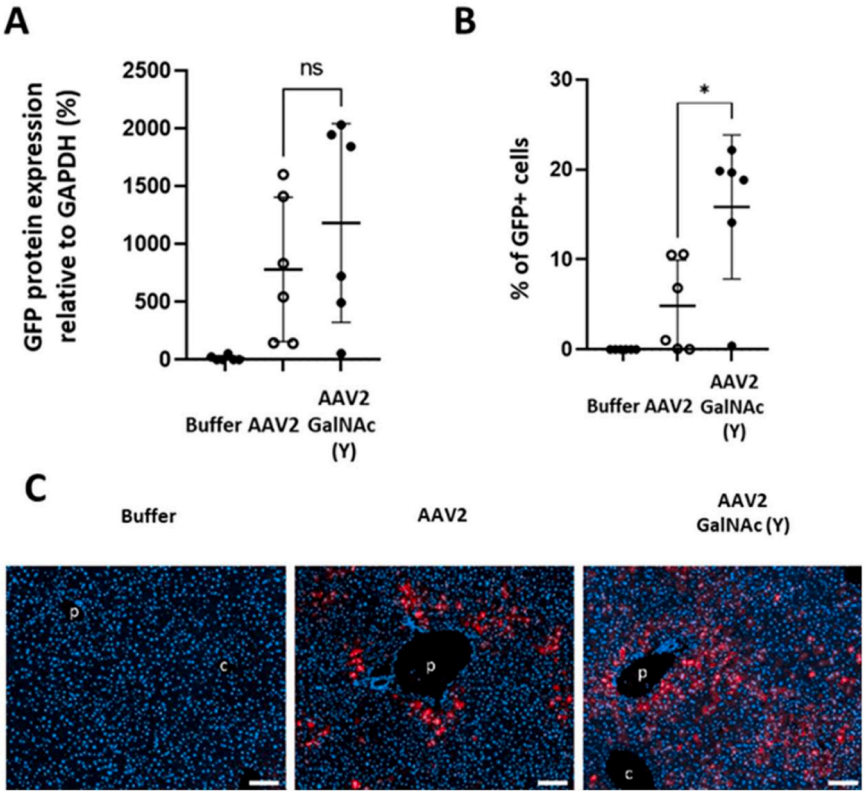

Fig. 3. A) Levels of GFP protein expression in mouse liver detected by Western blot 1 month after injection. B) Percentage of GFP-positive cells in liver, detected by GFP immunolabelling. C) Representative image of liver after GFP immunolabelling (red). p, portal vein branches; c, centro-lobular veins. DAPI counter-staining of nuclei is shown in blue. Scale bars= 200 μm.

same animals (**Table S-31**). These data show that, at the dose tested, Y-modification of rAAV2 does not increase the transduction of non-targeted tissues. Taken together, these findings indicate a positive impact of chemical Y modification of rAAV vectors for hepatocyte targeting *in vivo*. Increasing the number of transduced cells while decreasing vector copy number in these cells are both essential to overcome the efficacy and safety issues that limit the use of rAAV vectors for hepatic application.

The aim of this project was to develop vectors that can be modified according to the desired target. Therefore, we also used a mannose-derived ligand to generate rAAV2-Man(Y), and tested these vectors in retinal tissue, for which multiple gene therapy applications have been developed [39–41]. Prior to *in vivo* injection in the retina, infectivity of rAAV2-Man(Y) was evaluated by measuring the ratio of vector genomes (vg) to GFP-forming units (vg/GFU) in HEK293 cells [42]. This ratio is classically used as a quality control measure to evaluate the *in vitro* infectivity of rAAV vectors (the higher the ratio the lower the infectivity of the vector). The results showed that rAAV2-Man(Y) vector efficiently transduced HEK293 cells, and as observed for rAAV2-GalNAc(Y), rAAV2-Man(Y) was less infectious in the HEK293 cell line (Table S-32).

Retinal transduction efficiency of the modified capsid was next tested *in vivo* in adult wild-type C57/BL6 mice after subretinal injection of unmodified rAAV2 or rAAV2-Man(Y), both carrying the same CAG-eGFP expression cassette, and a control group was injected with buffer (n = 9 per group). *In vivo* fundus fluorescence performed one-month post-injection revealed higher intensity and more broadly distributed fluorescence (white dots) in mice injected with the modified capsid (Fig. S-33). The quantification of the fluorescence using a plugin in ImageJ software demonstrated a significant increase in the number of fluorescent objects and the overall density of fluorescence in the fundus after transduction of the retina with AAV2-Man(Y) *versus* the unmodified rAAV2 capsid (Fig. 4-A). To validate these *in vivo* findings, GFP fluorescence was evaluated in retinal flatmounts using confocal imaging. For this we distinguish between the region surrounding the injection site itself and the periphery or the region furthest from the injection site. The intensity and distribution of GFP fluorescence at the periphery of the injection site was higher in mice injected with rAAV2-Man(Y) *versus* unmodified rAAV2 (Fig. 4-B), suggesting increased diffusion of the former beyond the subretinal bleb induced by the injection. These data are in line with our observations in liver sections, whereby mice injected with rAAV2-GalNAC(Y) showed a broader distribution of GFP-positive cells. Furthermore, while GFP fluorescence around the injection site was comparable in rAAV2- and rAAV2-Man(Y)-transduced retinas at the level of outer segment (OS), outer nuclear layer (ONL), and inner nuclear layer (INL) (Fig. S-34), increased fluorescence intensity was observed in the ganglion cell layer (GCL) in all retinas injected with rAAV2-Man(Y) (Fig. 4-C). This suggests either greater rAAV2-Man(Y) uptake specifically in ganglion cells or better penetration of the vector through the tissue layers as a consequence of the mannose modification. This increased transduction efficiency in the GCL suggests that these mannose-modified vectors could be coupled with ganglion cell-specific promoters for gene therapy strategies targeting glaucoma or optic neuropathies [42,43].

Taken together, these data show that the rAAV2-Man(Y) capsid results in stronger and more widespread retinal transduction than the unmodified rAAV2 capsid.

4. Conclusion

Improvement of vector transduction efficiency is essential to overcome the many challenges implicit in rAAV gene therapy. Bioconjugation on the capsid itself may improve targeting, the efficiency of cell entry, and expression of the desired protein. By combining chemistry and vectorology, we have shown that specific ligands can be

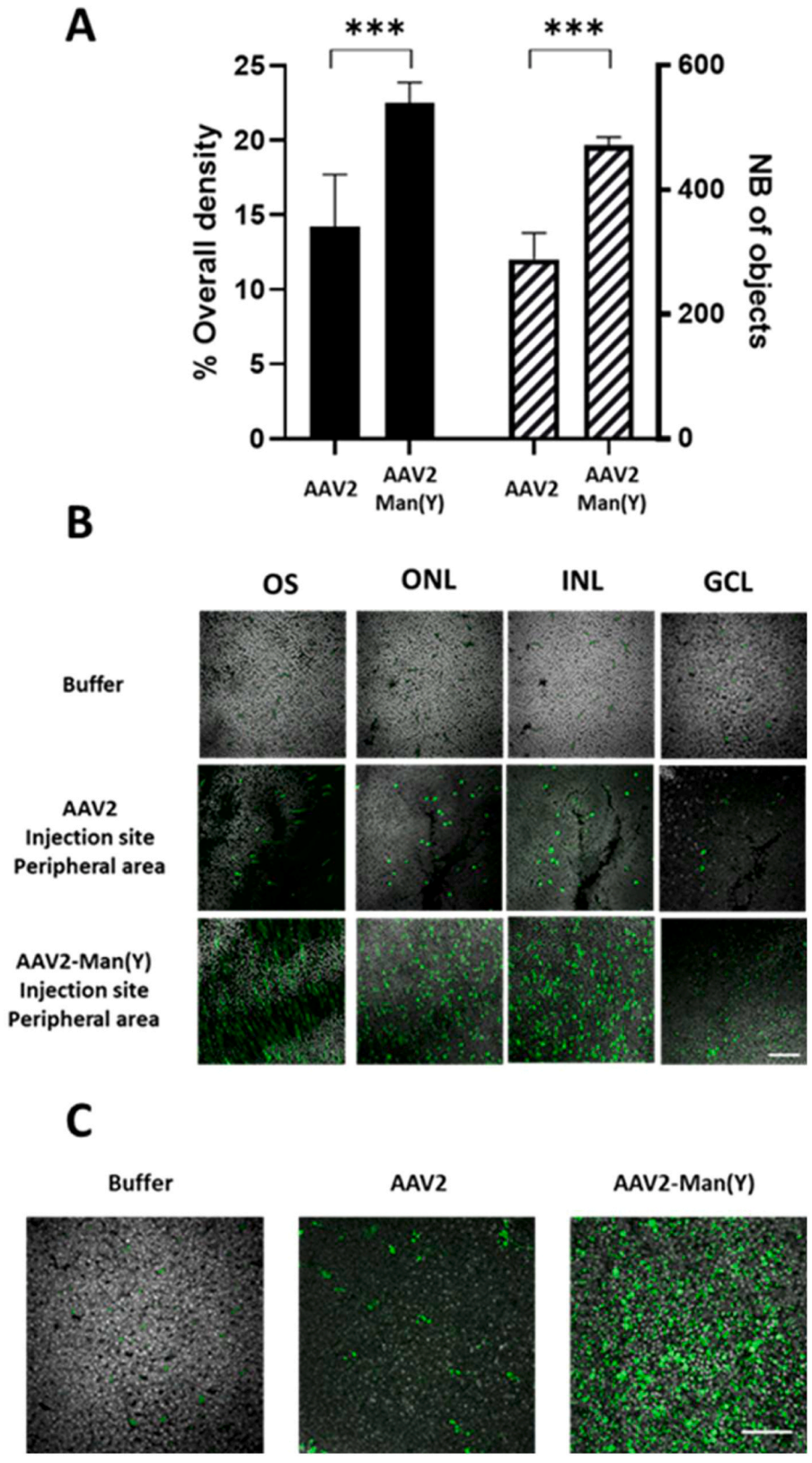

Fig. 4. GFP fluorescence study after subretinal injection. A) Quantification of GFP fluorescence in fundus images. Graphs depict the overall density of fluorescence (solid black bars) and number of fluorescent objects (hatched black bars). Both variables were significantly higher ($p = 0.0002$ and $p = 0.0008$ respectively) in mice injected with rAAV2-Man(Y) *versus* unmodified rAAV2. B) Representative confocal images of retinal flatmounts of mice injected with either buffer, rAAV2 or rAAV2-Man(Y) at the periphery of the injection site. Nuclei are stained in grey and GFP fluorescence is displayed in green (scale bar, 10 μm). OS: outer segments, ONL: outer nuclear layer, INL: inner nuclear layer, GCL: ganglion cell layer. C) Representative images of the ganglion cell layer at injection site of retinas injected with buffer, rAAV2, or rAAV2-Man(Y) are shown. Nuclei are stained in grey and GFP fluorescence is displayed in green (scale bar, 10 μm).

efficiently grafted onto Y residues of the native rAAV2 capsid. To the best our knowledge, this has never been done before.

Using our newly developed chemical capsid engineering platform we observed, both *in vitro* and *in vivo* in the liver and retina, a significant impact on vector transduction efficiency and expression of the gene of interest. In both targets, an increase in the area of transduction and the number of transduced cells was observed for tyrosine-modified *versus* unmodified rAAVs. Chemical remodeling of therapeutic viruses with diazonium salt may therefore constitute a valuable alternative to genetic engineering methods to improve organ tropism and protein expression in cells. In future studies, this technology will be evaluated with therapeutic transgenes for applications in the liver and retina and extended to other serotypes.

CRediT authorship contribution statement

Deniaud David: Writing – review & editing, Writing – original draft, Supervision, Resources, Methodology, Funding acquisition, Conceptualization. **Ducloyer Jean-Baptiste:** Visualization, Validation, Supervision, Methodology, Conceptualization. **Leray Aurélien:** Methodology, Conceptualization. **Mével Mathieu:** Writing – review & editing, Writing – original draft, Validation, Supervision, Funding acquisition. **Girard Tiphaine:** Methodology. **Lalys Pierre-Alban:** Methodology, Conceptualization. **Fraysse Bodvaël:** Software. **Varin Juliette:** Writing – original draft, Validation, Methodology, Conceptualization. **Ledevin Mireille:** Methodology, Formal analysis. **Bouzelha Mohammed:** Validation, Methodology, Conceptualization. **Adjali Oumeya:** Writing – review & editing, Writing – original draft, Resources, Project administration, Funding acquisition. **Depienne Sébastien:** Visualization, Methodology, Conceptualization. **Larcher Thibaut:** Writing – original draft, Supervision, Methodology, Conceptualization. **Marchand Maia:** Methodology, Conceptualization. **Cronin Thérèse:** Writing – original draft, Visualization, Methodology, Conceptualization. **Mellet Anthony:** Methodology. **Le Guiner Caroline:** Writing – review & editing, Writing – original draft, Validation, Supervision. **Demilly Joanna:** Validation, Methodology. **Guilbaud Mickaël:** Writing – original draft, Methodology, Formal analysis, Conceptualization. **Gouin Sébastien G.:** Writing – original draft, Supervision. **Alvarez-Dorta Dimitri:** Validation, Methodology. **Ayuso Eduard:** Visualization, Funding acquisition, Conceptualization. **Pavageau Karine:** Validation, Methodology. **Bourdon Audrey:** Writing – original draft, Validation, Supervision, Methodology, Conceptualization.

Declaration of Competing Interest

The authors declare the following financial interests/personal relationships which may be considered as potential competing interests: Mathieu MEVEL, David DENIAUD and Eduard AYUSO have patent licensed to rAAV vectors with chemically modified capsid

Data availability

Data will be made available on request.

Acknowledgments

The authors thank all personnel at the Boisbonne Center for Gene Therapy (ONIRIS, INSERM, Nantes, France) for handling and care of the rodents used in this study. We also thank the vector core of TaRGeT, UMR 1089 (CPV, INSERM and Nantes Université, which is a bioproduction and biotherapy national integrator (ANR-22-AIBB-0001), http://umr1089.univ-nantes.fr) for the production of the rAAV vectors used in this study. This research was supported by the Fondation d'Entreprise Thérapie Génique en Pays de Loire, the Centre Hospitalier Universitaire (CHU) of Nantes, the Institut National de la Santé et de la Recherche Médicale (INSERM), Nantes Université , and by grants from the French National Agency for Research ("Investissements d'Avenir" Equipex ArronaxPlus.n°ANR-11-EQPX-0004 and ChemAAV (ANR-19-CE18–0001)).

Appendix A. Supporting information

Supplementary data associated with this article can be found in the online version at doi:10.1016/j.biopha.2024.116148.

References

[1] H. Zhang, Q. Zhan, B. Huang, Y. Wang, X. Wang, AAV-mediated gene therapy: Advancing cardiovascular disease treatment, Front. Cardiovasc. Med. 9 (2022). https://www.frontiersin.org/articles/10.3389/fcvm.2022.952755 (Accessed 15 December 2022).
[2] J.M. Crudele, J.S. Chamberlain, AAV-based gene therapies for the muscular dystrophies, Hum. Mol. Genet 28 (2019) R102–R107, https://doi.org/10.1093/hmg/ddz128.
[3] N.J. Queen, X. Zou, J.M. Anderson, W. Huang, B. Appana, S. Komatineni, R. Wevrick, L. Cao, Hypothalamic AAV-BDNF gene therapy improves metabolic function and behavior in the Magel2-null mouse model of Prader-Willi syndrome, Mol. Ther. - Methods Clin. Dev. 27 (2022) 131–148, https://doi.org/10.1016/j.omtm.2022.09.012.
[4] E. Lunev, A. Karan, T. Egorova, M. Bardina, Adeno-associated viruses for modeling neurological diseases in animals: achievements and prospects, Biomedicines 10 (2022) 1140, https://doi.org/10.3390/biomedicines10051140.
[5] D.W. Russell, M.A. Kay, Adeno-associated virus vectors and hematology, Blood 94 (1999) 864–874.
[6] G. Le Meur, P. Lebranchu, F. Billaud, O. Adjali, S. Schmitt, S. Bézieau, Y. Péréon, R. Valabregue, C. Ivan, C. Darmon, P. Moullier, F. Rolling, M. Weber, Safety and long-term efficacy of AAV4 gene therapy in patients with RPE65 leber congenital amaurosis, Mol. Ther. 26 (2018) 256–268, https://doi.org/10.1016/j.ymthe.2017.09.014.
[7] W. Zhan, M. Muhuri, P.W.L. Tai, G. Gao, Vectored Immunotherapeutics for Infectious Diseases: Can rAAVs Be The Game Changers for Fighting Transmissible Pathogens? Front. Immunol. 12 (2021). https://www.frontiersin.org/articles/10.3389/fimmu.2021.673699 (Accessed 15 December 2022).
[8] U.T. Hacker, M. Bentler, D. Kaniowska, M. Morgan, H. Büning, Towards clinical implementation of adeno-associated virus (AAV) vectors for cancer gene therapy: current status and future perspectives, Cancers (Basel) 12 (2020) 1889, https://doi.org/10.3390/cancers12071889.
[9] J. Bennett, A.M. Maguire, Lessons learned from the development of the first FDA-approved gene therapy drug, voretigene neparvovec-rzyl, Cold Spring Harb. Perspect. Med (2022) a041307, https://doi.org/10.1101/cshperspect.a041307.
[10] H.A. Blair, Onasemnogene abeparvovec: a review in spinal muscular atrophy, CNS Drugs 36 (2022) 995–1005, https://doi.org/10.1007/s40263-022-00941-1.
[11] L. DeFrancesco, Drug pipeline 3Q22 — rare disease and Alzheimer's treatments, Nat. Biotechnol. 40 (2022) 1539–1541, https://doi.org/10.1038/s41587-022-01545-2.
[12] B.A. Hamilton, J.F. Wright, Challenges posed by immune responses to AAV vectors: addressing root causes, Front Immunol. 12 (2021) 675897, https://doi.org/10.3389/fimmu.2021.675897.
[13] T. Weber, Anti-AAV Antibodies in AAV gene therapy: current challenges and possible solutions, Front Immunol. 12 (2021) 658399, https://doi.org/10.3389/fimmu.2021.658399.
[14] C. Li, R.J. Samulski, Engineering adeno-associated virus vectors for gene therapy, Nat. Rev. Genet 21 (2020) 255–272, https://doi.org/10.1038/s41576-019-0205-4.
[15] A. Tantipanjaporn, M.-K. Wong, Development and recent advances in lysine and n-terminal bioconjugation for peptides and proteins, Molecules 28 (2023) 1083, https://doi.org/10.3390/molecules28031083.
[16] M. Mével, M. Bouzelha, A. Leray, S. Pacouret, M. Guilbaud, M. Penaud-Budloo, D. Alvarez-Dorta, L. Dubreil, S.G. Gouin, J.P. Combal, M. Hommel, G. Gonzalez-Aseguinolaza, V. Blouin, P. Moullier, O. Adjali, D. Deniaud, E. Ayuso, Chemical modification of the adeno-associated virus capsid to improve gene delivery, Chem. Sci. 11 (2019) 1122–1131, https://doi.org/10.1039/c9sc04189c.
[17] S. Depienne, M. Bouzelha, E. Courtois, K. Pavageau, P.-A. Lalys, M. Marchand, D. Alvarez-Dorta, S. Nedellec, L. Marín-Fernández, C. Grandjean, M. Boujtita, D. Deniaud, M. Mével, S.G. Gouin, Click-electrochemistry for the rapid labeling of virus, bacteria and cell surfaces, Nat. Commun. 14 (2023) 5122, https://doi.org/10.1038/s41467-023-40534-0.
[18] J.-B. Ducloyer, V. Pichard, M. Mevel, A. Galy, G.M. Lefevre, N. Brument, D. Alvarez-Dorta, D. Deniaud, A. Mendes-Madeira, L. Libeau, C. Le Guiner, T. Cronin, O. Adjali, M. Weber, G. Le Meur, Intravitreal air tamponade after AAV2 subretinal injection modifies retinal EGFP distribution, Mol. Ther. Methods Clin. Dev. 28 (2023) 387–393, https://doi.org/10.1016/j.omtm.2023.02.006.
[19] D. Alvarez Dorta, D. Deniaud, M. Mével, S.G. Gouin, Tyrosine conjugation methods for protein labelling, Chem. Eur. J. 26 (2020) 14257–14269, https://doi.org/10.1002/chem.202001992.
[20] S. Depienne, D. Alvarez-Dorta, M. Croyal, R.C.T. Temgoua, C. Charlier, D. Deniaud, M. Mével, M. Boujtita, S.G. Gouin, Luminol anchors improve the electrochemical-tyrosine-click labelling of proteins, Chem. Sci. 12 (2021) 15374–15381, https://doi.org/10.1039/d1sc04809k.

[21] Q.-Y. Hu, M. Allan, R. Adamo, D. Quinn, H. Zhai, G. Wu, K. Clark, J. Zhou, S. Ortiz, B. Wang, E. Danieli, S. Crotti, M. Tontini, G. Brogioni, F. Berti, Synthesis of a well-defined glycoconjugate vaccine by a tyrosine-selective conjugation strategy, Chem. Sci. 4 (2013) 3827–3832, https://doi.org/10.1039/C3SC51694F.
[22] E.J. Choi, D. Jung, J.-S. Kim, Y. Lee, B.M. Kim, Chemoselective tyrosine bioconjugation through sulfate click reaction, Chem. – A Eur. J. 24 (2018) 10948–10952, https://doi.org/10.1002/chem.201802380.
[23] T.L. Schlick, Z. Ding, E.W. Kovacs, M.B. Francis, Dual-surface modification of the tobacco mosaic virus, J. Am. Chem. Soc. 127 (2005) 3718–3723, https://doi.org/10.1021/ja046239n.
[24] X. Qiu, X. Kang, J. Zhu, L. Yi, Chemical labeling and crosslinking of tobacco mosaic virus via multi-diazonium reagents: examples, applications, and prospects, Mater. Adv. 3 (2022) 5248–5259, https://doi.org/10.1039/D2MA00311B.
[25] H. Büning, A. Srivastava, Capsid modifications for targeting and improving the efficacy of AAV vectors, Mol. Ther. - Methods Clin. Dev. 12 (2019) 248–265, https://doi.org/10.1016/j.omtm.2019.01.008.
[26] R. Nakahama, A. Saito, S. Nobe, K. Togashi, I.K. Suzuki, A. Uematsu, K. Emoto, The tyrosine capsid mutations on retrograde adeno-associated virus accelerates gene transduction efficiency, Mol. Brain 15 (2022) 70, https://doi.org/10.1186/s13041-022-00957-0.
[27] L. Zhong, B. Li, C.S. Mah, L. Govindasamy, M. Agbandje-McKenna, M. Cooper, R. W. Herzog, I. Zolotukhin, K.H. Warrington, K.A. Weigel-Van Aken, J.A. Hobbs, S. Zolotukhin, N. Muzyczka, A. Srivastava, Next generation of adeno-associated virus 2 vectors: point mutations in tyrosines lead to high-efficiency transduction at lower doses, Proc. Natl. Acad. Sci. 105 (2008) 7827–7832, https://doi.org/10.1073/pnas.0802866105.
[28] L. Zhong, B. Li, G. Jayandharan, C.S. Mah, L. Govindasamy, M. Agbandje-McKenna, R.W. Herzog, K.A. Weigel-Van Aken, J.A. Hobbs, S. Zolotukhin, N. Muzyczka, A. Srivastava, Tyrosine-phosphorylation of AAV2 vectors and its consequences on viral intracellular trafficking and transgene expression, Virology 381 (2008) 194–202, https://doi.org/10.1016/j.virol.2008.08.027.
[29] H.T. Le, Q.C. Yu, J.M. Wilson, M.A. Croyle, Utility of PEGylated recombinant adeno-associated viruses for gene transfer, J. Control Release 108 (2005) 161–177, https://doi.org/S0168-3659(05)00337-8 [pii] 10.1016/j.jconrel.2005.07.019.
[30] G.K. Lee, N. Maheshri, B. Kaspar, D.V. Schaffer, PEG conjugation moderately protects adeno-associated viral vectors against antibody neutralization, Biotechnol. Bioeng. 92 (2005) 24–34, https://doi.org/10.1002/bit.20562.
[31] S. D'Costa, V. Blouin, F. Broucque, M. Penaud-Budloo, A. François, I.C. Perez, C. Le Bec, P. Moullier, R.O. Snyder, E. Ayuso, Practical utilization of recombinant AAV vector reference standards: focus on vector genomes titration by free ITR qPCR, Mol. Ther. Methods Clin. Dev. 5 (2016) 16019, https://doi.org/10.1038/mtm.2016.19.
[32] C.Le Guiner, P. Moullier, V.R. Arruda, Biodistribution and shedding of AAV vectors, Methods Mol. Biol. 807 (2011) 339–359, https://doi.org/10.1007/978-1-61779-370-7_15.
[33] O. Pieroni, A. Fissi, J.L. Houben, Reaction of diazonium salt with tyrosine residues in polypeptides, Die Makromol. Chem. 176 (1975) 3201–3209, https://doi.org/10.1002/macp.1975.021761106.
[34] O. Khorev, D. Stokmaier, O. Schwardt, B. Cutting, B. Ernst, Trivalent, Gal/GalNAc-containing ligands designed for the asialoglycoprotein receptor, Bioorg. Med. Chem. 16 (2008) 5216–5231, https://doi.org/10.1016/j.bmc.2008.03.017.
[35] M. Mével, V. Pichard, M. Bouzelha, D. Alvarez-Dorta, P.-A. Lalys, N. Provost, M. Allais, A. Mendes, E. Landagaray, J.-B. Ducloyer, A. Galy, N. Brument, G.M. Lefevre, S.G. Gouin, C. Isiegas, G.L. Meur, T. Cronin, C.L. Guiner, M. Weber, P. Moullier, E. Ayuso, D. Deniaud, O. Adjali, Mannose-coupled AAV2: a second generation AAV vector for increased retinal gene therapy efficiency, (2022) 2022.12.01.518481. https://doi.org/10.1101/2022.12.01.518481.
[36] D. Boyle, L.F. Tien, N.G. Cooper, V. Shepherd, B.J. McLaughlin, A mannose receptor is involved in retinal phagocytosis, Invest Ophthalmol. Vis. Sci. 32 (1991) 1464–1470.
[37] M. Tanowitz, L. Hettrick, A. Revenko, G.A. Kinberger, T.P. Prakash, P.P. Seth, Asialoglycoprotein receptor 1 mediates productive uptake of N-acetylgalactosamine-conjugated and unconjugated phosphorothioate antisense oligonucleotides into liver hepatocytes, Nucleic Acids Res 45 (2017) 12388–12400, https://doi.org/10.1093/nar/gkx960.
[38] J. O'Donnell, K.A. Taylor, M.S. Chapman, Adeno-associated virus-2 and its primary cellular receptor—Cryo-EM structure of a heparin complex, Virology 385 (2009) 434–443, https://doi.org/10.1016/j.virol.2008.11.037.
[39] J.-B. Ducloyer, G. Le Meur, T. Cronin, O. Adjali, M. Weber, Gene therapy for retinitis pigmentosa, Med Sci. (Paris) 36 (2020) 607–615, https://doi.org/10.1051/medsci/2020095.
[40] M. Pavlou, C. Schön, L.M. Occelli, A. Rossi, N. Meumann, R.F. Boyd, J.T. Bartoe, J. Siedlecki, M.J. Gerhardt, S. Babutzka, J. Bogedein, J.E. Wagner, S.G. Priglinger, M. Biel, S.M. Petersen-Jones, H. Büning, S. Michalakis, Novel AAV capsids for intravitreal gene therapy of photoreceptor disorders, EMBO Mol. Med. 13 (2021) e13392, https://doi.org/10.15252/emmm.202013392.
[41] I. Trapani, P. Tornabene, A. Auricchio, Large gene delivery to the retina with AAV vectors: are we there yet? Gene Ther. 28 (2021) 220–222, https://doi.org/10.1038/s41434-020-0174-4.
[42] M. Lock, S. McGorray, A. Auricchio, E. Ayuso, E.J. Beecham, V. Blouin-Tavel, F. Bosch, M. Bose, B.J. Byrne, T. Caton, J.A. Chiorini, A. Chtarto, K.R. Clark, T. Conlon, C. Darmon, M. Doria, A. Douar, T.R. Flotte, J.D. Francis, A. Francois, M. Giacca, M.T. Korn, I. Korytov, X. Leon, B. Leuchs, G. Lux, C. Melas, H. Mizukami, P. Moullier, M. Muller, K. Ozawa, T. Philipsberg, K. Poulard, C. Raupp, C. Riviere, S.D. Roosendaal, R.J. Samulski, S.M. Soltys, R. Surosky, L. Tenenbaum, D.L. Thomas, B. van Montfort, G. Veres, J.F. Wright, Y. Xu, O. Zelenaia, L. Zentilin, R.O. Snyder, Characterization of a recombinant adeno-associated virus type 2 reference standard material, Hum. Gene Ther. 21 (2010) 1273–1285, https://doi.org/10.1089/hum.2009.223.
[43] K.S. Hanlon, N. Chadderton, A. Palfi, A. Blanco Fernandez, P. Humphries, P. F. Kenna, S. Millington-Ward, G.J. Farrar, A Novel Retinal Ganglion Cell Promoter for Utility in AAV Vectors, Front. Neurosci. 11 (2017). https://www.frontiersin.org/articles/10.3389/fnins.2017.00521 (Accessed 19 January 2023).